Verification of a 2D wave model

Eduardo Nunes Lima
eduardo.n.lima@tecnico.ulisboa.pt

Instituto Superior Técnico, Universidade de Lisboa, Portugal

January 2020

Abstract

A verification study is done for the simulation of water wave propagation in a 2D open domain with regards to the main wave quantities. This study is done using ReFRESCO, a CFD code developed by MARIN that captures the free surface location using the VOF method. The end goal of this dissertation is to contribute to standardized procedures in wave simulation. The statistical errors – regarding to the influence of the initial condition on the wave – and numerical errors – regarding the iterative and discretization errors – are assessed for two wave models in deep water conditions: a linear wave and a 5th order Stokes. The numerical set up in terms of grid topology and absorption conditions are based on the available literature. The wave quantities of interest are assessed in two ways: at a fixed location in space, by averaging the quantities in time and by analysing the moving wave through the domain. This work presents a study comparing the discretization of three convective schemes regarding robustness, accuracy and computational costs. The influence of the interpolation of the free surface location on the different quantities of interest is investigated throughout this work. The relation between the wave dispersion errors and the wave reflection at the outlet of the domain is established, with the reflection having two separated components: one dependent on the discretization errors and another dependent on the relation between wave model and boundary condition.

Keywords: Wave Simulation, Solution Verification, Wave Reflection, Computational Fluid Dynamics, Volume of Fluid

1. Introduction

Numerical wave simulation, namely using CFD (Computational Fluid Dynamics) codes, is usually required in many practical hydrodynamic problems to describe the complex underlying flow physics. The use of numerical simulation in engineering applications needs to be accompanied by systematic exercises of Verification and Validation of the numerical solution in order to avoid incorrect solutions or inadequate model choices. Validation concerns quantifying the modelling errors, while Verification is a mathematical problem with two activities: Code Verification – to verify the absence of errors in the code – and Solution Verification – to estimate the error and uncertainty of a given solution.

In this work, a Solution Verification study is done on a 2D wave propagating in an empty domain using ReFRESCO [1], a Finite-Volume CFD code developed by MARIN in collaboration with several non-profit organizations. The mathematical equations solved are the Navier-Stokes equation. The flow is assumed to be laminar and so the equations do not require any statistical treatment to handle turbulent fluctuations. ReFRESCO makes use of the Volume of Fluid (VOF) method to accurately capture the FS; the formulation of this method is presented in [2].

When simulating waves in deep water conditions, one of the main concerns is to avoid wave reflection. Several studies have addressed this issue, see $e.g.$ [3], [4]. Absorption effectiveness tests are presented in [4] and [5], where optimal parameters are recommended.

Regarding Verification and Validation exercises, a detailed example of a Code Verification on wave propagation can be seen in [6], while [5] presents a Verification and Validation study on a problem involving wave simulation. The Verification done in this work addresses the influence of the numerical and statistical error. The influence of the iterative error is assessed by evaluating the changes in the solution with different iterative tolerances; the statistical error is evaluated by studying the influence of the total simulated time and the number of waves used in computing the average values of the quantities of interest; the convergence of relevant wave properties using grid and time step refinement is done to estimate the discretization error and the solution uncertainty, and to analyse its effects on the simulated wave.

The main properties of the two waves compared in this work are presented in table 1.

Wave properties	Linear	5^{th}order Stokes
Wave height [m]	1.5	24
Period [s]	12.56	12.56
Wavelength [m]	246.55	266.38
Steepness	0.006	0.09

Table 1: Main wave properties from two different waves compared in this work.

2. Numerical errors and uncertainty

The numerical error can be divided into three main categories: iterative errors, discretization errors, and round-off errors.

The round-off errors are the result of the finite precision of computers. This type of error is several orders of magnitude below other sources, thus they are not addressed in this work. The iterative errors derive from the non-linear mathematical models solved by CFD. This work focuses on the residuals of the non-linear solution procedure as a method of monitoring the iterative error. Regarding the discretization error, this is usually the dominant type of numerical error. The estimation of the exact solution is done using is a grid and time step convergence study. The estimation of the discretization error using power series expansion on unsteady flow is given by:

$$\epsilon_\phi \approx \phi_i - \phi_0 = \alpha_x h_i^{p_x} + \alpha_t \tau_i^{p_t}, \qquad (1)$$

where the subscript 0 corresponds to the estimation of the exact solution and i corresponds to the solution of a given grid; α_x and α_t are constants; h is the typical cell size; τ is the time step size, and p_t and p_x are the observed order of convergence in time and space, respectively. If the discretization error is the dominant error source and the refinement is sufficiently fine, then the observed order of convergence should be equal to the order of discretization of the numerical models. In practical applications, scatter results may influence the observed convergence due to many factors: from the complex nature of the equations being solved to the to noise introduced by the post-processing techniques employed to obtain the solution. These factors influence the observed orders of convergence.

The estimation of the numerical uncertainty defines an interval that should contain the exact solution with 95% of confidence; this interval is defined as :

$$\phi_i - U_\phi \leq \phi_{\text{exact}} \leq \phi_i + U_\phi. \qquad (2)$$

The guidelines for the discretization error estimation and the quantification of the solution's uncertainty are given in detail in [7]. In this work, these procedures are applied using the tool Numerical Uncertainty Analysis, developed by MARIN, that is available at [8].

3. Simulation settings

3.1. Numerical schemes

This work compares two schemes in regards to time discretization and three schemes in regards to convective flux discretization. The discretization in time is done using Implicit Three Time-Level (first-order accurate) and Implicit Euler (second-order accurate). In the discretization of the convective flux, we compared three schemes: QUICK (Quadratic Upstream Interpolation for Convective Kinematics), limited QUICK, and Harmonic. Their formulation can be seen in [9], [10] and [11], respectively. Finally, the discretization of the VOF transport equation is done using REFRICS, an interface-capturing scheme that is discussed in detail in [2].

The monitoring of the wave elevation is accomplished by tracking the FS location at every time step. ReFRESCO has built-in monitors for this purpose. The VOF field is defined between 0 and 1, corresponding respectively to the water and air phases. These wave-probe monitors interpolate the VOF field to locate the interface. In this case, the interface is defined by $\alpha = 0.5$, following the common procedure seen, e.g., in [12]. In this work, three interpolation settings are compared: Barycentric type 2 and 3, with the monitors aligned with the cell centres, and also Barycentric type 2 with the locations non-aligned

3.2. Generation and absorption boundary conditions (GABC)

The waves generation is done by prescribing the velocity and the volume-fraction fields at the boundary cells.

The absorption techniques can be divided into two categories: boundary-based and domain-based absorption. The boundary-based (also denominated as non-reflective) make use of the Sommerfeld condition to absorb the wave. The boundary-based techniques used in this work are known as body forces. This technique uses the source terms in the momentum conservation equations and on the VOF transport equation to gradually force the flow to match the prescribed wave. The intensity of the body forces is controlled by a function that guarantees its progressive application; the detailed description of this technique can be seen in [4]. These two techniques are used simultaneously in this work: the body forces to force the solution to the analytical solution and then the Sommerfeld boundary condition absorbs the outgoing wave.

3.3. Grid topology and grid refinement

This work adopts the same grid topology principle seen in [4] regarding the wave energy-based topology. However, this is adapted to Cartesian structured grids. The horizontal refinement is independent of the $y-$direction and it is equidistant. The water region underneath the FS is divided into two regions: zone A' and zone B', that can be seen in figure 1. The vertical refinement in Zone A' is equidistant, while in Zone B' the refinement is defined using a stretching function. The first cell from Zone B' has $\Delta y_{\text{Zone A'}} = \Delta y_{\text{Zone B'}}$. The Δy progressively increases towards the domain bottom. The refinement of the air region is symmetrical to that of the water region.

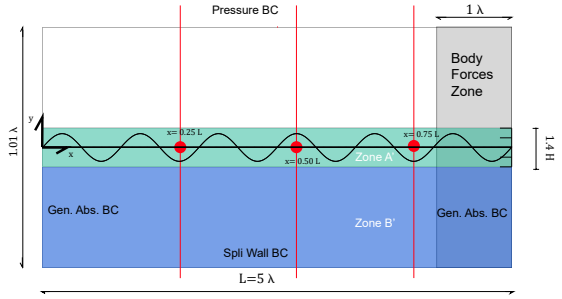

Figure 1: general grid topology and set up used in this work.

Figure 1 shows the baseline topology for this work, as well as the location and types of BC. It also shows the location of the forcing zone and the location of the monitors used to record the wave elevation. The box in Zone A', is made 40 % higher than the wave height. This dimension is set to guarantee a fine cell size in FS and at its vicinity. The use of Cartesian structured grids has two advantages: first, it eliminates the error from non-orthogonality and eccentricity corrections; second, it easier to guarantee geometrically similar grids. Nonetheless, the drawbacks regarding this type of grids are the total number of cells.

The grids and time steps used throughout this work are summarized in tables 2 and 3. The grids in table 2 have the same number of cells in both Cartesian directions. In the $x-$ direction, the cells are equidistant, meaning that all the cell size have the same horizontal cell size. The values of CFL presented in table 3 are obtained relative to the maximum CFL value observed for a simulation using grid B and $dt = T/184$.

The grid chosen for the baseline simulation settings is grid B, with the time step dt_B for a CFL of 0.12. These baseline settings are equivalent to coarse settings used in the literature.

[1] This dimension corresponds to the total height of Zone A'

Grid	h_i/h_0	#/ (1.4H) [*1]	#/λ	total #
Grid A	4	9	21	11 025
Grid B	3	12	28	19 600
Grid C	2	18	42	44 100
Grid D	1	36	96	176 400

Table 2: Grids used in the convergence study.

CFL number	dt_A	dt_B	dt_C	dt_D
0.12	T/184	T/245	T/368	T/736
0.25	T/88	T/118	T/177	T/353
0.5	T/44	T/59	T/89	T/177

Table 3: Time step used convergence study. The value in the denominator is approximated to the unit. The subscripts in the time steps correspond to the grids in 2.

4. Post-Processing Methods

To have a more complete analysis of the wave characteristics, the wave elevation is analysed in two ways: at a fixed location within a given time interval and also across an array of monitors equally spaced in the domain and aligned with the direction of propagation.

The quantities of interest used to characterize the wave at a fixed location are the wave height ($\overline{\text{H}}_t$) and period ($\overline{\text{T}}_t$). These wave characteristics are averaged for a set N waves.

The monitor array is used to determine the wave height as a function of the domain position $\text{H}(x_i)$ – where x_i is the location of each monitor. This approach can be described as the recording of the wave height of the last simulated wave to fully propagate from the inlet to the outlet of the domain. The use of the last simulated wave in this analysis is done to guarantee that the transient effects are minimized. The reflection coefficient (Cr_x), the average height along the domain ($\overline{\text{H}}_x$), the wave diffusion, the wavelength ($\overline{\lambda}$) and wave the phase shift ($\Delta\phi$) are all computed from the $\text{H}(x_i)$ function.

Following the approach used in [13], the reflection coefficient used in this work is given by:

$$\text{Cr} = \frac{\text{H}_{\text{max}} - \text{H}_{\text{min}}}{\text{H}_{\text{max}} + \text{H}_{\text{min}}} \tag{3}$$

The reflection coefficient (Cr_x) is evaluated using $\text{H}(x_i)$. The reflection coefficient is then computed between the maximum ($\text{max} < \text{H}(x_i) >$) and minimum ($\text{min} < \text{H}(x_i) >$) in the domain section comprised between $2\lambda < x < 4\lambda$. Further details of the post-processing methods can be seen in [14].

5. Verification studies: Iterative and statistical error

This section provides an overview of the influence of the iterative error and the statistical treatment of the quantities of interest. The simulations in this section are performed for the baseline settings (grid B and dt_B with a total number of cells of 19600 cells). The wave quantities of interest evaluated in this section are the average wave height $\overline{H}_t$ and period $\overline{T}_t$.

5.1. Iterative error

The influence of the iterative error in the solution is addressed with regards to an adequate choice of an iterative criterion tolerance. This is accomplished with an tolerance convergence study to determine its sensitivity of the solution to the iterative error. The choice of the iterative criterion tolerance has a significant impact on the computational cost. Five simulations with different L_∞ tolerance criteria are compared. The lowest tolerance used is 10^{-6} and the highest is 10^{-2}. The simulated time corresponds to 60 periods. This simulated time guarantees minimal impact of statistical error in quantities of interest.

Linear			
L_∞	$(\overline{H}_t - \overline{H}_{t\ 10^{-6}})/\overline{H}_{t\ 10^{-6}}$		
	25% L	50% L	75% L
10^{-2}	1.395×10^{-3}	3.188×10^{-3}	4.433×10^{-3}
10^{-3}	2.281×10^{-4}	4.476×10^{-4}	6.249×10^{-4}
10^{-4}	3.778×10^{-5}	9.993×10^{-4}	1.041×10^{-5}
10^{-5}	8.340×10^{-5}	1.878×10^{-4}	2.216×10^{-4}

Stokes			
L_∞	$(\overline{H}_t - \overline{H}_{t\ 10^{-6}})/\overline{H}_{t\ 10^{-6}}$		
	25% L	50% L	75% L
10^{-2}	7.555×10^{-6}	1.007×10^{-5}	2.424×10^{-5}
10^{-3}	2.294×10^{-7}	1.974×10^{-6}	1.991×10^{-6}
10^{-4}	1.378×10^{-7}	2.511×10^{-9}	9.514×10^{-7}

Table 4: Relative differences of the data values for $\overline{H}_t$ between the different criterion using 10^{-6} solution as a reference, where *i* stands for each tolerance and *L* stands for the domain length.

The results from the iterative convergence are shown in table 4, where the results are presented as the difference to the value obtained with the lowest tolerance ($L_\infty = 10^{-6}$). For the linear wave, some of the table entries for the tolerances lower than $L_\infty = 10^{-4}$ presented values where the difference between the solutions is greater than the tolerance. In this cases, the iterative criterion does not reflect the level of iterative error. For the Stokes wave, this study shows that all relative differences between the solutions are at least one order of magnitude lower when compared with the linear wave. The results of $\overline{T}_t$ for both wave models are omitted given that they were two orders of magnitude below the $\overline{H}_t$ values.

From this results it can be seen that an increase in CPU time does not justify the gain in accuracy achieved by using tolerances beyond 10^{-3}. Thus, $L_\infty = 10^{-3}$ is the tolerance used throughout this work.

5.2. Statistical uncertainty

The estimated statistical uncertainty is the interval around the averaged value that reflects the variation in the values of the sample. It is given by:

$$U_N = \frac{1}{N}\sqrt{\sum_{i=1}^{N}(\phi_i - \overline{\phi})^2}, \tag{4}$$

where ϕ_i is a value from the sample, $\overline{\phi}$ is the average value and N is the sample size. The waves included in the sample are schematically represented in figure 2. Figure 3 shows the successive differences of the wave quantities of interest for the linear wave. It can be seen that, in both cases, the waves are influenced by the initial condition and that this influence became negligible after 30 to 35 periods of simulation. After this, the quantities maintain the same differences. The Stokes wave demonstrated the same tendencies. However, its values were one order of magnitude higher. Thus, to evaluate the statistical uncertainty, the following scenarios were considered: using a short simulation time (30 periods) and by using a long simulation time (120 in the linear wave and 60 for the Stokes wave). The estimated uncertainty is evaluated regarding the sample size in these two scenarios. The results are shown in table 5.

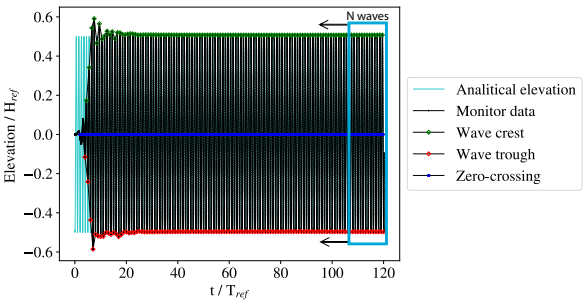

Figure 2: Linear wave elevation for 120 periods of simulation

For the linear wave, the results demonstrate that the lowest statistical uncertainty is attained for the longer simulated time with a sample size around 20 waves. However, the absolute value of the uncertainty of $\overline{H}_t$ for 30 simulated periods with a sample size of 5 waves is in the same order of magnitude of iterative tolerance criterion ($L_\infty = 10^{-3}$). We can conclude that the computational costs associated with the 120 periods of simulated time would not

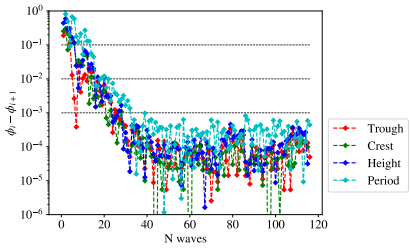

Figure 3: Successive differences for 120 period of simulation for the linear wave.

Linear			
Sample size		Simulated time	
		120 T	30 T
#5	H/H_{ref}	1.005	1.006
	U/H_{ref}[%]	8.474×10^{-4}	6.787×10^{-2}
#10	H/H_{ref}	1.004	1.009
	U/H_{ref}[%]	9.121×10^{-4}	1.562×10^{-1}
#20	H/H_{ref}	1.004	1.015
	U/H_{ref}[%]	6.495×10^{-4}	2.775×10^{-1}

Stokes			
Sample size		Simulated time	
		60 T	30 T
#5	H/H_{ref}	0.867	0.868
	U/H_{ref}[%]	4.503×10^{-4}	8.807×10^{-2}
#10	H/H_{ref}	0.867	0.872
	U/H_{ref}[%]	3.001×10^{-4}	1.873×10^{-1}
#20	H/H_{ref}	0.867	0.877
	U/H_{ref}[%]	4.291×10^{-4}	2.757×10^{-1}

Table 5: Comparison between long and short simulation time lengths with three sample sizes for the two waves.

significantly increase the precision of the calculation done in this work. As for the Stokes wave, the results show that the uncertainty for the shortest simulation is around 0.02% of H_{ref} for a sample of 5 waves. In terms of absolute value, this figure is just slightly above the iterative tolerance. From these results, we can conclude that the settings used in the linear wave in terms of the statistical uncertainty and iterative convergence yield similar consequences in both wave models. In this case, the values of $\overline{T}_t$ were one order of magnitude below $\overline{H}_t$. This is consistent with the trend observed for iterative errors. The values of the period can be seen in [14]. The simulations done throughout this work use a simulated time of 30 periods and $\overline{H}_t$ and $\overline{T}_t$ are obtained with a sample size of 5 waves.

6. Verification studies: Grid and time step convergence studies

The grid and time step convergence studies presented were done to addresses the influence of the discretization error in the simulation of the linear wave and compare different numerical schemes with regards to robustness, computational cost and accuracy. The convergence of the Stokes wave was done only with the numerical scheme that yielded better results.

The results of the convergence of $\overline{H}_t$ for the centre of the domain are shown in figures 4, 5, 6. The results of the convergence show that the first-order accuracy in time integration penalizes the error level of $\overline{H}_t$. The convergence in figure 4(a) reflects the numerical diffusion present in this simulation. It can be seen that α_t from equation 1 is greater than α_x. On the other hand, the convergence of the Stokes wave in figure 6(c) presents a significant slope in α_x, which indicates that the space discretization error is the dominant factor in the convergence.

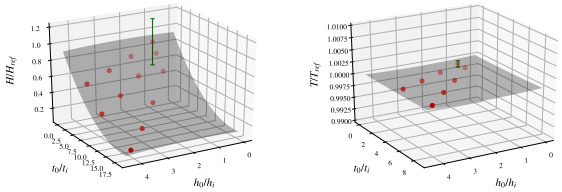

(a) Average wave height. $\phi_0 = 8.814 \times 10^{-1}$, $U_{\phi_1} = 49.0\%$. (b) Average wave period. $\phi_0 = 1.0002$, $U = \%0.0$.

Figure 4: Linear wave: convergence of $\overline{H}_t$ and $\overline{T}_t$ for CFL of 0.12 and 0.25 and 0.5 with Implicit Euler and QUICK.

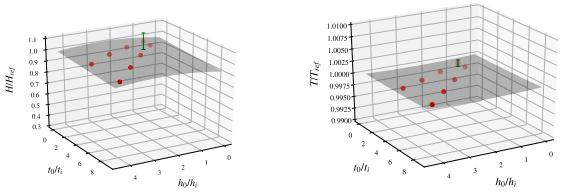

(a) Average wave height. $\phi_0 = 9.722 \times 10^{-1}$, $U_{\phi_1} = 11.18\%$. (b) Average wave period. $\phi_0 = 1.0002$, $U = \%0.0$.

Figure 5: Linear wave: convergence of $\overline{H}_t$ and $\overline{T}_t$ for CFL of 0.12 and 0.25 for Three Time Level with QUICK.

The results of the convergence have shown that the influence of the discretization errors on $\overline{T}_t$ was negligible given that the values of the uncertainty are significantly lower than those of $\overline{H}_t$. This is observed independently of the wave model, convective scheme and accuracy in time integration. These results are consistent with the trend observed for iterative and statistical errors.

The convergence for three domain location is shown in 7. These results show that the conver-

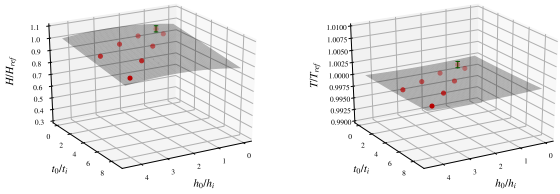

(a) Linear wave average height. (b) Linear wave average period. $\phi_0 = 9.791 \times 10^{-1}$, $U = 3.81\%$. $\phi_0 = 1.0002$, $U = \%0.0$.

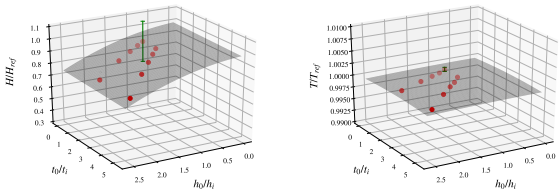

(c) Stokes wave average height. $\phi_0 = 9.975 \times 10^{-1}$, $U = 17.7\%$. (d) Stokes wave average period. $\phi_0 = 9.9983 \times 10^{-1}$, $U = 0.0\%$.

Figure 6: Convergence of wave height and period for linear and Stokes waves with Three Time Level and limited QUICK schemes.

gence has different tendencies and estimated exact values depending on the location. Nonetheless, they are all consistent, i.e., there is overlap between all error bars. Other noise factors like monitor interpolation error, post-processing and wave reflection play a role in the convergence.

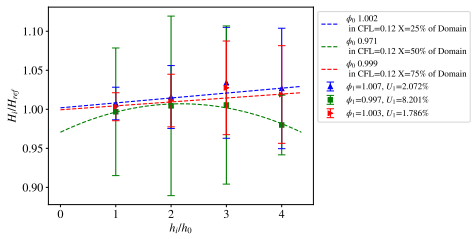

Figure 7: Convergence of CFL=0.12 line for three domain locations: 25, 50 and 75 % of L.

6.1. Comparison between QUICK, limited QUICK and Harmonic

Figure 8 shows the wave height convergence for the QUICK and limited QUICK, and for the Harmonic and limited QUICK schemes. In the first case, the two schemes present different fitting curves; the uncertainty for QUICK is lower given it presents a monotonic convergence.

Finally, the convective schemes were also compared regarding robustness and the computational cost. In each of these aspects, the limited QUICK performed better than the other two schemes.

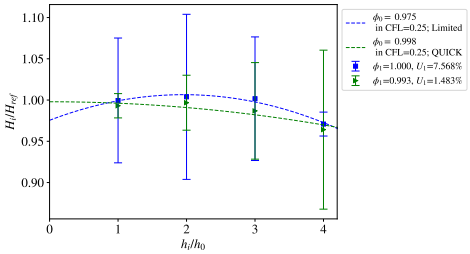

(a) QUICK and Limited QUICK

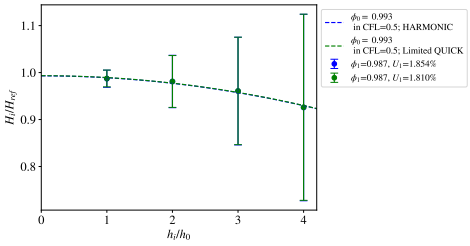

(b) Harmonic and Limited QUICK

Figure 8: Comparison between schemes on the convergence of $\overline{H}_t$ at 50 % of L

6.2. Sensitivity study

Table 6 presents the sensitivity study done for the two waves. The baseline grid and time step parameters are the same for both waves, however, the linear wave was subjected to a higher refinement level given its lower sensitivity to the numerical parameters when compared with the Stokes wave. It can be seen that the most significant changes in both waves were introduced by the refinement in the $x-$direction, i.e., the wave propagation direction.

Linear		
Variables	$\overline{\lambda}/\lambda_{ref}$	$\overline{H}_t/H_{ref}$
Baseline simulation	0.985	1.006
$1.5 \times y-$direction	0.985	0.993
$1.5 \times x-$direction	0.989	1.016
$1.5 \times t$	0.984	1.000

Stokes		
Variable	$\overline{\lambda}/\lambda_{ref}$	$\overline{H}_t/H_{ref}$
Baseline Simulation	1.031	0.868
$1.25 \times y-$direction	1.033	0.851
$1.25 \times x-$ direction	1.025	0.911
$t/1.25$	1.033	0.868

Table 6: Summary of numerical properties for the sensitivity study, for the linear wave

7. Convergence of the main wave properties

This section provides a comparison of the two wave models regarding the convergence of the main wave properties analysed using $H(x)$. This study was done for a single CFL line of 0.12. The objective

of this discussion is to see how the influence of the numerical error relates to wave models and their simulation settings and to see the interpolation error. The wave reflection, which is an indirect consequence of the discretization error, is also analysed.

Each quantity is assessed with three monitor interpolation settings. In one setting, 100 equally spaced monitors are placed throughout the domain, independently of the grid refinement. In the other two, the monitors are aligned with the cell centres (in the vertical direction) and the number of monitors changes with the grid refinement; the difference between this two monitors is the interpolation scheme. Since the FS is interpolated by these monitors, this allows us to see the influence of the FS interpolation on the convergence of these quantities.

7.1. Average wave height

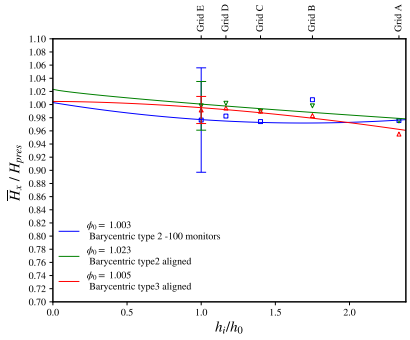

(a) $\overline{H}_x$ of the linear wave

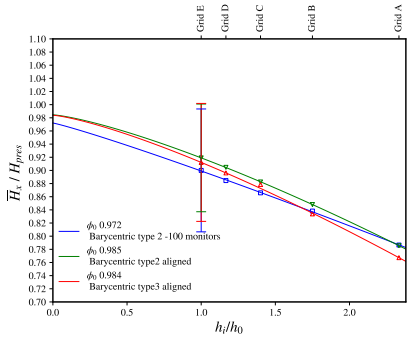

(b) $\overline{H}_x$ of the 5th order Stokes wave

Figure 9: Average wave height convergence for the two wave models. The error bars represent the numerical uncertainty and the values on the legend correspond to the estimated exact solution.

The convergence of the average wave height in figure 9 shows a significant influence of the monitor interpolation has a significant influence on the $\overline{H}_x$. This influence is reflected in the different tendencies of the fitting curves.

The levels of uncertainty are higher for the Stokes wave despite the small difference between the data points and the fitting curve. The main factor that contributes to this is the difference between the estimated error and the data point of the finest grid.

Comparing the quantities of interest in both wave models, it can be concluded that the numerical diffusion plays an important role in the simulation of the Stokes waves and that this effect shapes the fitting curves. As for the linear wave, it can be seen that its data points are more sensitive to the noise factors present in the simulation.

7.2. Average wavelength ($\overline{\lambda}$) and phase error ($\Delta\phi$)

The $\overline{\lambda}$ value is computed considering the whole domain except the region of application of the body forces. This value is computed at the last time step of the simulation. The deterioration of wave propagation is reflected in the difference between $\overline{\lambda}$ and the reference value. However, $\overline{\lambda}$ is not an accurate measure to evaluate the dispersion error of the wave at the vicinity of the outlet boundary condition. $\Delta\phi$ is used for this purpose.

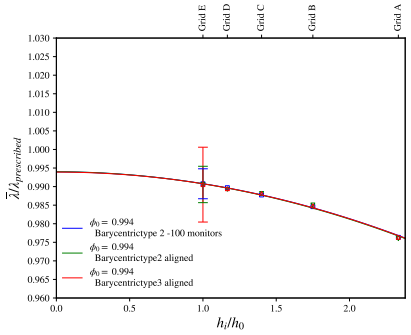

(a) $\overline{\lambda}$ from linear wave

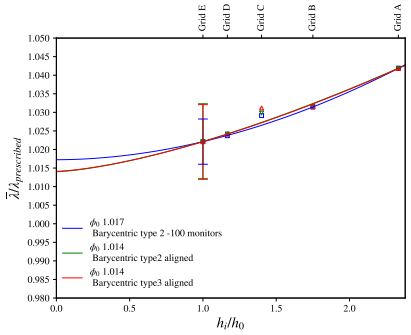

(b) $\overline{\lambda}$ from 5th order Stokes wave

Figure 10: Average wavelength convergence for the two wave models.

The convergence if $\Delta\phi$ indicates that the dispersion error implies a decrease in the wavelength of the linear wave, while it produces the opposite effect in the Stokes wave. This can be seen in figure 10. The tendencies observed in these results are similar to the convergence in the exercise done in [6] for the Stokes and the linear waves.

The measuring of $\Delta\phi$ is done in the vicinity of the

body forces region. The results are presented in figure 11 in terms of the percentage of one wave period. As discussed previously, the period is not influenced by the refinement, thus an increase in wavelength implies an increase in the wave propagation velocity and consequently the wave phase. This relation justifies why $\Delta\phi$ decreases with the increase of the refinement level while also displaying a similar tendency in the fitting curve that of the $\overline{\lambda}$.

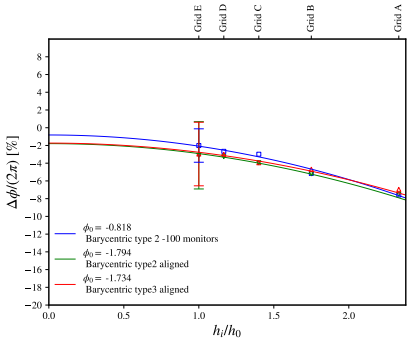

(a) $\Delta\phi$ from linear wave

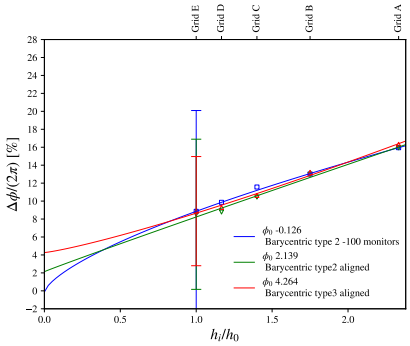

(b) $\Delta\phi$ from 5th order Stokes wave

Figure 11: Phase error convergence for the two wave models.

7.3. Reflection coefficient

The study of the reflection coefficient quantifies the reflection of the wave at the and absorption conditions: Sommerfeld BC and the body forces. Cr is computed applying equation 3 to the wave height along the domain – H(x) .

The convergence of Cr, presented in figure 12, shows that the Cr decreases with the refinement level. In figure 12(b) the fitting was done without the grid A given that this data points were clearly diverging from the fitting tendency of the rest of the data points. This is divergence is likely to be a consequence of the wave diffusion in that diminishes the amplitude of the reflected wave.

For the linear wave, the estimated exact solution is less the 0.5 % whereas for the Stokes wave the estimated exact solution is between $2.35\% < Cr_x < 2.48\%$. These results show that the Stokes

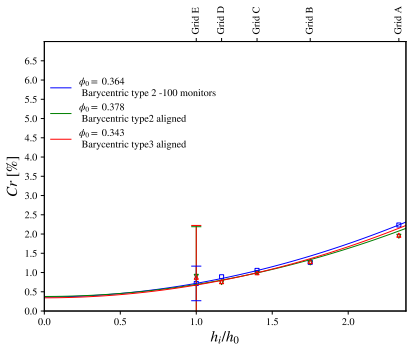

(a) Linear wave Cr

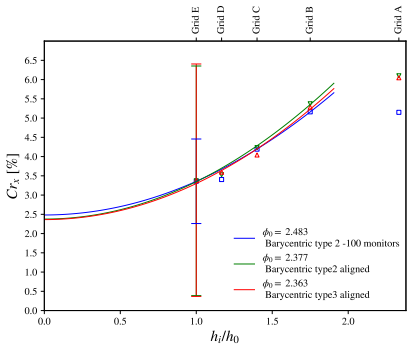

(b) 5th order Stokes wave Cr

Figure 12: Reflection coefficient convergence for the two wave models.

wave tends to Cr significantly higher than that of the the linear wave. This difference was also observed on a convergence study on the Stokes wave condition in [6] , however in this example no body forces had been applied to the wave. This fact suggests that the difference seen between Cr in the exact solution is due to an error introduced by the Sommerfeld BC.

To confirm the influence of Sommerfeld BC, three simulations of the Stokes without body forces were done. The results are presented in table 7.

Grid	$Cr_{\text{Sommerfeld}}$ [%]	Δ_{Cr}[%]
Grid B	1.673	3.698
Grid C	2.105	2.082
Grid D	2.344	1.060
ϕ_0	2.921	0.55

Table 7: Cr of the Stokes wave using only the Sommerfeld boundary condition at the outlet. $\Delta_{Cr} = |Cr_{\text{Sommerfeld}} - Cr_{baseline}|$ is the difference between the solution with and without body forces.

Table 7 show the difference between the Cr obtained with and without body forces (Δ_{Cr}). It is shown that Δ_{Cr} decrease with the increase in the refinement level. As the difference between the setups resides only on the presence of the body

forces, then this factor must be the source of the added Cr contribution.

The convergence of Cr for the linear wave further reinforces this two mentioned reflection sources since Cr presents an estimated value close to zero. This indicates that when the body forces component decreases with the refinement level and the wave is fully absorbed by the Sommerfeld boundary condition. Hence, it can be concluded that there is one reflection component that is a function of the discretization error, which is linked to the body forces and another that is a function of the wave model itself which is associated with the Sommerfeld boundary condition. The wave reflection can then be summarized by the equation:

$$Cr = Cr_{\text{sommerfeld}} + Cr_{\text{body forces}}, \tag{5}$$

8. Conclusions

This work presents a Solution Verification study for regular wave propagation in an open domain. Two waves provided by two different wave models were compared under deep water conditions. The quantities of interest of the wave were analysed considering the statistical error as well as the numerical error and its consequences on the propagating wave. The following conclusions were drawn from the results obtained in this work:

- The study on the influence of the iterative error, monitored by the residuals L_∞ norm, showed that the gain in accuracy with a tolerance beyond 10^{-3} did not justify the increase in CPU time.
- Regarding the initial condition, it can be neglected for a simulation time greater than 30 to 35 periods of simulation.
- The results of the study on the statistical uncertainty showed that the lowest uncertainty was obtained for longer simulated times for both waves. Nevertheless, the absolute value of the uncertainty for 30 periods with 5 waves in the sample is in the same order of the iterative tolerance ($L_\infty = 10^{-3}$). Despite displaying the same tendency, the Stokes' wave uncertainty for the 30 simulated periods was around 0.02% of H_{ref} for a sample of 5 waves. In terms of absolute value, this figure is just slightly above the iterative tolerance that was set.
- The influence of the numerical error on the wave period was significantly lower than on the wave height. On the iterative and statistical error, the error for the period was at least one order bellow the error for the wave height. Regarding the discretization error, it was seen that it had a negligible effect on $\overline{T}_t$ on the simulations using second-order accurate schemes for the discretization of the time terms.
- The convergence of grid and time step using Implicit Euler showed that using a first-order accurate scheme in time penalises the solution. The results show a significant wave diffusion that makes this scheme unsuited for this type of applications.
- The grid and time step convergence showed that different domain locations presented different fitting curves and estimated values. This demonstrates the presence of noise factors that influence the convergence, such as interpolation errors and wave reflection.
- In the sensitivity study done to $\overline{\lambda}$ and $\overline{H}_t$, it was demonstrated that Stokes wave has a greater sensitivity to the changes in the grid parameters than the linear wave. Furthermore, the refinement in the wave propagation direction proved to be the most significant parameter. Thus, a greater refinement in this direction is recommended to improve the quality of theses type of simulations.
- From the convergence of $\overline{H}_x$, the three interpolation schemes used yielded three different fitting curves with on both waves. However, this influence was more pronounced on the linear wave given the influence of the diffusion in the Stokes wave convergence.
- The convergence of the $\overline{\lambda}$ and $\Delta\phi$ it is observed the same tendencies on the fitting curves.
- Regrading the reflection, it was concluded that two factors are contributing to the reflected wave: the body forces and the wave model. Regarding the body forces, it was seen that this contribution tends to zero with the increase in the refinement level, while the contribution related to the wave model tends to a fixed value.

References

[1] Refresco web page. http://www.refresco.org.

[2] C. M. Klaij, M. Hoekstra, and G. Vaz. Design, analysis and verification of a volume-of-fluid model with interface-capturing scheme. *Computers and Fluids*, 170:324–340, 2018.

[3] Robinson Perić. Analytical prediction of reflection coefficients for wave absorbing layers. (November), 2017.

[4] Stéphane Rapuc, Pierre Crepier, Frédérick Jaouen, Tim Bunnik, and Pauline Regnier. Towards guidelines for consistent wave propagation in CFD simulations. *NAV International*

Conference on Ship and Shipping Research, (221499):515–524, 2018.

[5] Simon Burmester and Guilherme Vaz. Towards credible CFD simulations for floating offshore wind turbines. *Ocean Engineering*, 209(January):107237, 2020.

[6] Fahd Fathi, Luís Eça, and Mart Borsboom. An example of code verification in the simulation of wave propagation. *Proceedings of the International Conference on Offshore Mechanics and Arctic Engineering - OMAE*, 6:313–321, 2011.

[7] L. Eça and M. Hoekstra. A procedure for the estimation of the numerical uncertainty of CFD calculations based on grid refinement studies. 262.

[8] Verification and validation utilities/tools, 2020.

[9] Joel H. Ferziger Milovan Peric. *Computacional Methods for fluid dynamics*. third edition.

[10] N. P. Waterson and H. Deconinck. Design principles for bounded higher-order convection schemes - a unified approach. *Journal of Computational Physics*, 224(1):182–207, 2007.

[11] Martin Hoekstra. *Numerical simulation of ship stern flows with a space-marching Navier-Stokes method*. PhD thesis, Delft University of Technology.

[12] Luís Eça, Guilherme Vaz, and Martin Hoekstra. Code verification, solution verification and validation in rans solvers. 49149:597–605, 2010.

[13] F. Ursell, R. G. Dean, and Y. S. Yu. Forced small-amplitude water waves: A comparison of theory and experiment. *Journal of Fluid Mechanics*, 7(1):33–52, 1960.

[14] Eduardo Lima. Verification of a 2d wave model. Master's thesis, Instituto Superio Técnico, 2021.